Design and Simulation of a Fuel Cell-based Hybrid Underwater Vehicle Propulsion System in Matlab/Simulink

Huy Chien Nguyen
School of Mechanical Automotive Engineering, Hanoi University of Industry, Vietnam
chiennh@haui.edu.vn (corresponding author)

Nguyen Ha Hiep
Institute of Vehicle and Energy Engineering, Le Quy Don Technical University, Vietnam
hahiepshippower@lqdtu.edu.vn

Received: 19 April 2024 | Revised: 2 May 2024 and 6 May 2024 | Accepted: 14 May 2024

 DOI: https://doi.org/10.48084/etasr.7550

ABSTRACT

Remotely Operated Vehicles (ROVs) and Autonomous Underwater Vehicles (AUVs) have many applications in underwater missions. A recurring issue is managing the power source of the vehicle, especially air-independent propulsion sources, such as batteries, accumulators, and fuel cells, to increase diving depth, underwater endurance, and range. The current article proposes the use of both fuel cells and batteries simultaneously. The subject of the study is Pluto Plus ROVs, which are mine sweeping and counter-terrorism underwater vehicles. The considered system is simulated in Matlab/Simulink. The result was a block diagram that simulates a hybrid propulsion system for submersibles in general and serves as the basis for improving the propulsion system for Pluto Plus ROVs.

Keywords-fuel cell; battery; propulsion; simulation; hybrid propulsion system

I. INTRODUCTION

Although oceans cover more than 70% of the Earth's surface, more than 95% of their area remains unexplored [1]. The use of Underwater Vehicles (UVs) is an ideal solution for expanding the range of tasks in undersea exploration. Unmanned UV (UUVs) are small UVs that operate underwater without direct human control. These include Remotely Operated Vehicles (ROVs) and Autonomous UVs (AUVs). UUVs often use battery propulsion systems or hybrid propulsion systems of batteries and Fuel Cells (FCs) [2-6]. FCs, especially Proton-Exchange Membrane Fuel Cells (PEMFC) supplied with hydrogen and oxygen, have higher performance, are small, lightweight, easy to handle, and are able to operate at lower temperatures (below 100 °C) [8-11]. Combined propulsion system PEMFCs with lithium-ion batteries are ideal for UVs. The need to create highly efficient hybrid propulsion based on FCs attracts a growing number of developers and researchers, who work on designing, modeling, and manufacturing hybrid propulsion. Research can be carried out through (1) experimental study, (2) analytical investigation, and (3) modeling and simulations. Experimental studies [12-15] were performed without numerical calculations, which is a time-consuming and expensive process. Analytical investigation, which involves adjusting input parameters to calibrate analytical results to coincide with the experimental data, can be complicated. Numerical modeling and simulations play an essential role in developing hybrid propulsion systems because they shed light on how different components in the system influence its performance and make it possible to tune the parts, while optimizing size and mass to increase the underwater operating range and endurance of UVs [16-23]. This study designed and simulated an FC-based hybrid propulsion system applied to a UV that uses pure battery propulsion systems. In order for this to be achieved, it was necessary to solve some problems, such as calculating the UV movement resistance, determining the propulsion power, and computing the power of the FC and the battery. Models of the system components were built in the Matlab/Simulink environment. The system operation was simulated to obtain parameters that serve as input for model calibration and completion of the hybrid system. This work serves as the basis for designing and producing an actual hybrid system.

II. MATERIALS AND METHODS

A. Research Object

The research object is the Pluto Plus ROV, which is employed to locate, inspect, and clear underwater targets. The main characteristics of Pluto Plus ROV are [7, 24]: dimensions of 2250 × 580 × 770 mm, weight of 320 kg, maximum carrying capacity of 100 kg, maximum speed of 6 knots, calculated speed of 3.5 knots, maximum diving depth of 400 m, underwater endurance at 6 knots of 2 h.

B. Calculations of Propulsion System Power

The calculation is based on viscous resistance using the viscous resistance coefficient C_V, the friction resistance coefficient C_F, and the shape factor $(1 + k)$:

$$C_F = 0.075 / (\log Re - 2)^2 \quad (1)$$

where $Re = vL/\mu$, μ is the kinematic viscosity of seawater [m^2/s], L is the length of the ROV [m], and v is its speed [m/s].

The shape factor can be obtained from the Droblenkov curve for a UUV with a circular cross section [25]:

$$(1+k) = 1 + 0.2(D/L) + 8(D/L)^2 - 10(D/L)^3 \quad (2)$$

where D is the diameter of the ROV [m], considering the average width and height. Thus, the viscous resistance is calculated by [25]:

$$R_V = \rho \Omega v^2 C_V / 2 = \rho \Omega v^2 C_F (1+k) / 2 \quad (3)$$

where ρ = 1025 [kg/m^3] is the density of seawater, Ω is the wet surface area of the ROV (a cylinder of diameter D and length L).

The required power is calculated by (4) where η_D is the propeller efficiency:

$$N_p = vR_v / \eta_D \quad (4)$$

From (3) and (4), we have:

$$N_p = \left[\rho \Omega C_F (1+k) / (2\eta_D)\right] v^3 \quad (5)$$

The inputs for the calculations are presented in Table I.

TABLE I. INPUT DATA FOR CALCULATIONS

Parameter	Value	Unit	Parameter	Value	Unit
μ	$1.57.10^{-6}$	m^2/s	T	0.58	m
v	3.5	knots	D	0.675	m
	1.543	m/s	B	0.77	m
L	2.25	m	η_D	0.4	-

Based on Table I, and (1)-(5), the curve in Figure 1 shows the relationship between the required power and speed. With a speed of v = 3.5 knots, the power N_p = 222.7 W, whereas with v_{max} = 6 knots, N_p = 1011 W. To ensure that the FCs work best, it is necessary for the types of losses due to transmission to be added. The rated power to calculate for the FC is 300 W.

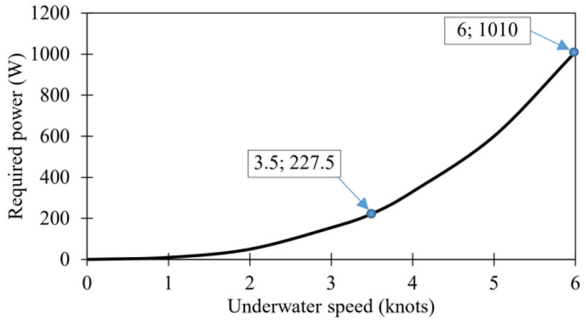

Fig. 1. The dependence of propulsion power on the ROV speed.

C. The Proposed Hybrid Propulsion System

Pluto Plus ROV only utilizes batteries (Figure 2), so there are many limitations regarding range and endurance. Therefore, the proposed model installed with PEMFCs will limit these disadvantages [8].

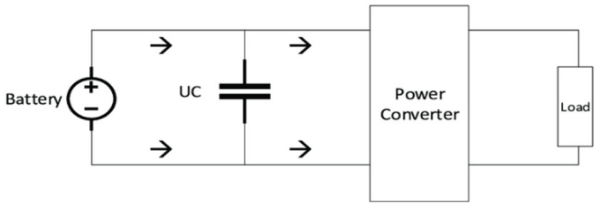

Fig. 2. Power scheme of the original Pluto Plus ROV.

The proposed FC-based hybrid propulsion system for the Pluto Plus ROV is depicted in Figure 3. With the proposal to install FCs as the main energy source besides the battery, through the above calculation parameters, the power of FCs generated is 300 W, corresponding to the nominal speed of 3.5 knots.

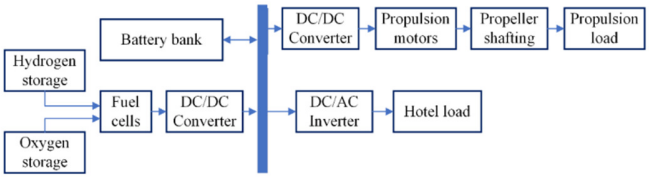

Fig. 3. The proposed fuel cell-based hybrid propulsion system.

D. Calculation of FC Parameters

Energy is obtained in an FC from thermodynamic energy through electrochemical reactions inside the FC. Basically, the energy acquired from the exothermic reaction forms water from H_2 and O_2. The energy is attained by enthalpy ΔH (kJ/mol), which is broken down into thermal energy by specific entropy ΔS (kJ/mol.K) multiplied by the absolute temperature T, and the electricity is Gibbs free energy ΔG (kJ/mol) [22]:

$$\Delta H = \Delta G + T\Delta S \quad (6)$$

$$W_{el} = \Delta G = -QE = -nFE \quad (7)$$

where W_{el} is the electrical useful work, determined by the amount of electricity Q [C] and potential E [V], n = 2 is the number of electrons transferred for each molecule of fuel consumed and F is Faraday's constant (96487 C/mol).

$$E = -\Delta G / nF = -(\Delta H - T\Delta S) / nF \quad (8)$$

This value may vary with the working temperature, the partial pressure of the reactants and the resulting products relative to the reference condition (T_{ref} = 25 °C, P_{refv} = 1 atm). The effect of temperature changes when considering ΔH and ΔS constants and is calculated by [22]:

$$\Delta E = (\Delta S / nF)(T - T_{ref}) \quad (9)$$

The partial pressure change affects ΔG because G is a function of the specific volume V (m^3/mol) and the change in

pressure dP (i.e. $G = V.dP$). From the gas law $V = RT/P$, we have:

$$\Delta G = \Delta G^o - (RT / nF)\ln(P_{H_2}^1 P_{O_2}^{0.5} / P_{H_2O}^1) \quad (10)$$

where ΔG^o = -237.17 kJ/mol is the Gibbs free energy at standard conditions and R = 8.3143 J/(mol.K).

In (10), consider an FC working on pure hydrogen with a partial pressure of P_{H_2} and pure oxygen with a partial pressure of P_{O_2}, so the potential of the FC is [23]:

$$\begin{aligned} &E_{Nerst} = -\Delta G^o / nF + \Delta S\left(T - T_{ref}\right)/nF + \\ &RT\ln\left(p_{H_2}^1 p_{O_2}^{0.5} / p_{H_2O}^1\right)/nF = 1.23 - \\ &0.85\cdot10^{-3}(T - 298.15) + 4.31\cdot10^{-5}T\ln\left(p_{H_2}^1 p_{O_2}^{0.5} / p_{H_2O}^1\right) \end{aligned} \quad (11)$$

where the partial pressure values are calculated by:

$$\log p_{H_2O} = -2.1794 + 0.02953t$$
$$-9.1837\cdot10^{-5}t^2 + 1.4454\cdot10^{-7}t^3$$
$$p_{H_2} = 0.5P_{H_2} / \exp\left(1.653 i_{FC} / T^{1.334}\right) - p_{H_2O}$$
$$p_{O_2} = P_{O_2} / \exp\left(4.192 i_{FC} / T^{1.334}\right) - p_{H_2O}$$

Equation (11) is the Nerst equation, which gives the maximum possible potential. There are four types of losses in FCs:

- Active losses: this kind of losses is necessary, like a spark, to initiate reactions. It depends on temperature, partial pressure, and catalyst on the electrodes [22]:

$$V_{act} = -\left[\xi_1 + \xi_2 T + \xi_3 T\ln(C_{o2}) + \xi_4 T\ln(i_{FC})\right] \quad (12)$$

where ξ_i is a coefficient, i_{FC} is the FC amperage [A], and C_{O2} is the concentration of oxygen on the catalyst surface [mol/cm^3].

$$C_{O_2} = p_{O_2} / 5.08\cdot10^6 \cdot \exp(-498/T) \quad (13)$$

- Ohmic losses: this kind of losses is caused by the resistance of the proton exchange membrane and the resistance due to the contact between the electrode and the membrane surface as well as the electrode surface with the bipolar plates and the collector plates [23]:

$$V_{ohm} = i_{FC}.(R_m + R_c) \quad (14)$$

$$R_m = \rho_m l / A \quad (15)$$

where R_c is the constant resistance of the cell, R_m is the temperature-dependent resistance, l is the thickness of the membrane [cm], A is the active area of the membrane [cm^2], ρ_m is the specific resistance of the membrane (Ω.cm), determined by (16), where parameter Ψ expresses the degree of membrane hydration (with a value of 14 if the membrane is fully hydrated and 23 if the membrane is oversaturated) [23]:

$$\rho_m = \frac{181,6\cdot\left[1 + 0,03\cdot\left(\frac{i_{FC}}{A}\right) + 0,062\cdot\left(\frac{T}{303}\right)^2\cdot\left(\frac{i_{FC}}{A}\right)^{2,5}\right]}{\left[\Psi - 0,634 - 3\left(\frac{i_{FC}}{A}\right)\right]\cdot\exp\left[\frac{4,18(T-303)}{T}\right]} \quad (16)$$

- Concentration losses or mass transfer losses: They express the mass transfer limit of the reactants. Although feeding reactants at high speeds will give high current densities in the FC, there is a limit to the feed rate, and the reactants may not be used properly. The current density limit j_L is the maximum current density value that the FC can produce and is about 1.4 A/cm^2 [22, 23].

$$V_{conc} = -B\ln(1 - j / j_L) \quad (17)$$

where B is a coefficient depending on the operating conditions, j is the instantaneous current density (A/cm^2), and $j = i_{FC}/A$.

Finally, the formula for determining the FC potential is:

$$V_{cell} = E_{Nerst} - V_{act} - V_{ohm} - V_{conc} \quad (18)$$

The parameters for calculating PEMFC are didplayed in Table II [22, 23]. The cathode and anode inlet pressures are taken to be 60 psig (4.08 atm) according to [14], and the proton exchange membrane is Nafion-117. Combining (6)-(18) with Table II, the cell polarization curve $V_{cell} = f(j)$ of Figure 4 is constructed.

TABLE II. PARAMETERS FOR CALCULATING PEMFC

Parameter	Value	Unit	Parameter	Value	Unit
T	353	K	ζ_2	$3.12\cdot10^{-3}$	-
A	60	cm^2	Rc	0.0008	Ω
l	178.10^{-4}	cm	j_L	1.4	A/cm^2
P_{H2}	3	atm	ζ_3	$7.4.10^{-5}$	-
P_{O2}	3	atm	ζ_4	$-1.8.10^{-4}$	-
B	0.08	-	ψ	23	-
ζ_1	-0.96	-	-	-	-

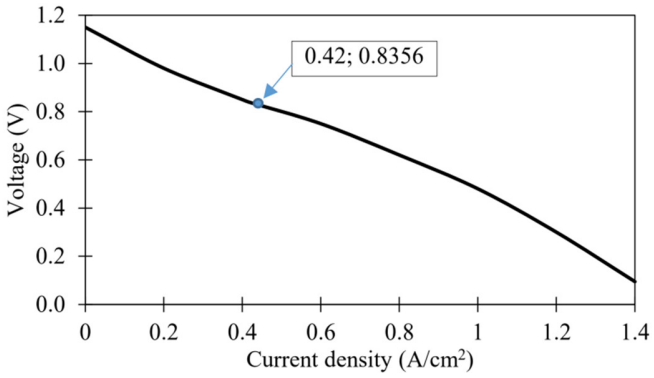

Fig. 4. Voltage-current characteristic of an FC.

The initial expected efficiency of the selected PEMFC was η = 0.57 and j = 0.42 A/cm^2 [10]. Thus, the output voltage of a cell is V_{cell} = 0.84 V. The current of the fuel cell stack is equal to the current density j multiplied by the operating area A_{cell} of the single cell. $I = jA_{cell}$ = 25 A. The output power of the FC stack is $P = UI$. Thus, with the known values, the generated voltage of the FC stack is $U = P/I$ = 12 V. The voltage U of the

stack consisting of n single cells connected in series is calculated by $U = nV_{cell}$. The value of n can be derived as: $n = U/V_{cell} = 14$ cells. The fuel cell calculating results are summarized in Table III.

TABLE III. FC STACK CALCULATION PARAMETERS

Parameter	Value	Unit
Number of single cell, n	14	cell
Current density, j	0.42	A/cm^2
Fuel cell stack power, P	300	W
Fuel cell stack current, I	25	A
Fuel cell stack voltage, U	12	V
Single cell voltage, V_{cell}	0.84	V

E. Simulation of a FC-based Hybrid Propulsion System

The hybrid system comprises two sources of energy: the PEMFCs and the battery. When the ROV operates at a speed below the rated one, the PEMFC generates electricity for the running propulsion system and charges the battery. When the ROV operates from the rated to the maximum speed, the PEMFC and the battery provide electrical power to the propeller's required power output. The process of building a hybrid system for simulating its dynamics consists of the following steps: (1) building a PEMFC model, (2) creating a battery bank model, (3) construction of a DC-DC boost converter, (4) connecting the system components, performing simulations, and calibrating their parameters.

The PEMFC parameters and model are manifested in Table IV and Figure 5, respectively. The battery bank is the "Batteries" block (Figure 6). The DC-DC boost converter is essential for the propulsion system by ensuring the required voltage for electric motors. The setting parameters for the PI controller are provided in Table V. To reduce the complexity in the simulation model, the whole DC-DC boost converter after its construction is reduced to a Subsystem located in the block diagram of the entire model (Figure 7). After building the components of the system, these parts are connected. The block diagram of the system simulation model is portrayed in Figure 8. A simulation is carried out according to the pre-established simulation time.

TABLE IV. INPUT PARAMETERS FOR THE PEMFC

Parameter	Value	Unit
Voltage at 0 A and 1 A, V_0, V_1	28; 26	V
Current at the end point, I_{end}	25.5	A
Voltage at the end point, V_{end}	11.74	V
Efficiency, η	0.57	-
Operating temperature, t	80	℃
Gas pressure H_2 supply, P_f	3	bar
Gas pressure O_2 supply, P_{Air}	3	bar
Percentage of H_2 gas in the container, x_{H_2}	1	-
Percentage of O_2 gas in the container, y_{O_2}	1	-
Percentage of H_2O vapor in the air, z_{H_2O}	0	-
Efficiency factor of H_2, $U_{f_{H_2}}$	0.8334	-
Efficiency factor of O_2, $U_{f_{O_2}}$	0.5004	-

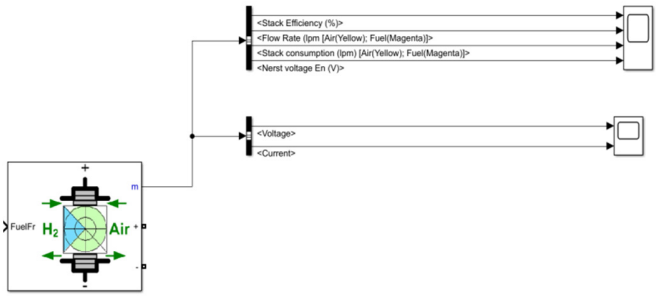

Fig. 5. The PEMFC model.

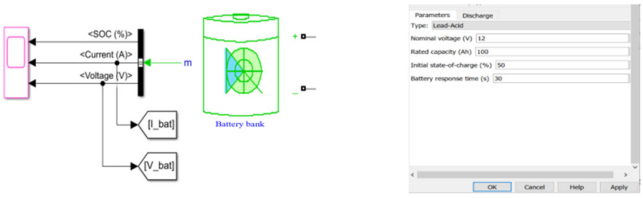

Fig. 6. Block "Batteries" and input parameters for the battery bank.

TABLE V. PI CONTROLLER PARAMETERS

Parameter	Value	Unit
Inductance, L	500.e^{-6}	H
Capacitor capacitance, C	7500.e^{-5}	F
PI controller parameter, r	0.2	Ω
Transferring function, $G(s)$	1/(0.0001 +1)	-
Coefficient K_P	0.005	-
Cofficient K_I	0.15	-
Voltage set, U_{ref}	24	V
Duty cycle, T_s	1.e^{-4}	s

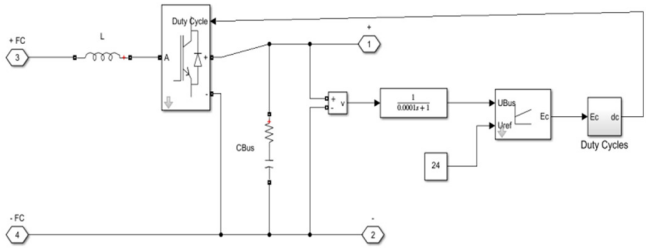

Fig. 7. DC-DC boost converter model.

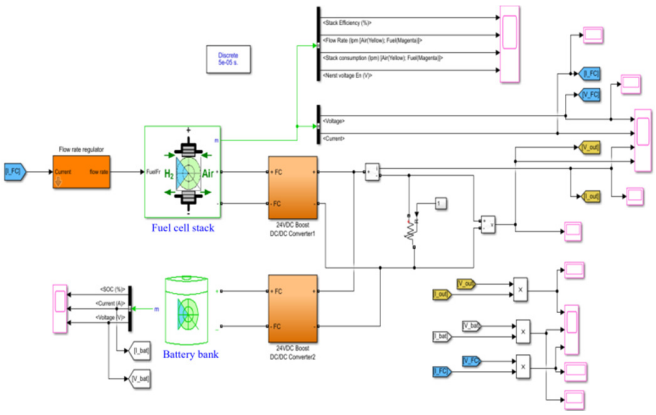

Fig. 8. Fuel cell-based hybrid propulsion system model.

III. RESULTS AND DISCUSSION

The simulation results are illustrated as a time-dependent graph in the Scope block (Figures 9-13). In addition, the Display option will disclose the stability parameters of the values for a working hybrid system compared to the set value.

The operating parameters of the PEMFC (efficiency, fuel consumption, oxygen consumption, voltage, current) (Figures 9, 10) and the battery bank (Figure 12) emerging by a numerical simulation correspond to the expected calculations. After system startup, the PEMFC power is maintained at a stable level of 300 W (Figure 11). The speed at t = 7.34 s corresponds to the nominal speed of the ROV (v = 3.5 knots), and up to this point, the PEMFC provides propulsion power to the ROV and simultaneously charges the battery. From 7.34 s and further, the power for the ROV is provided from PEMFC and a backup battery bank (Figures 11 and 12).

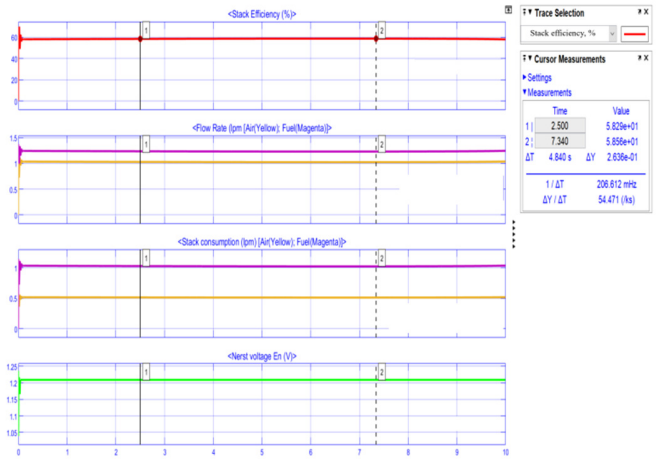

Fig. 9. Simulation results of PEMFC operating parameters.

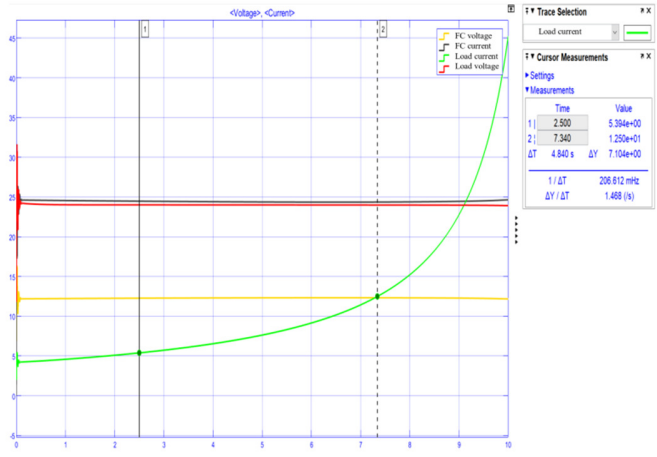

Fig. 10. Simulation results of PEMFC and load current and voltage.

According to Figure 10, the voltage and current of the PEMFC are stable at 12 V and 25 A, respectively, while the voltage drop on the propeller hybrid engine is also stable at 24 V. The change in load according to the vehicle propulsion power is the change in the upper current applied to the electric motor. When the ROV speed changes the values may change slightly. Figure 13 depicts the power components of the fuel cell-based hybrid propulsion system changing according to the alteration in the speed of the ROV, thereby observing the power coordination of the energy sources, which is the basis for building a controller. It automatically combines or divides the power of the fuel cell-based hybrid propulsion system.

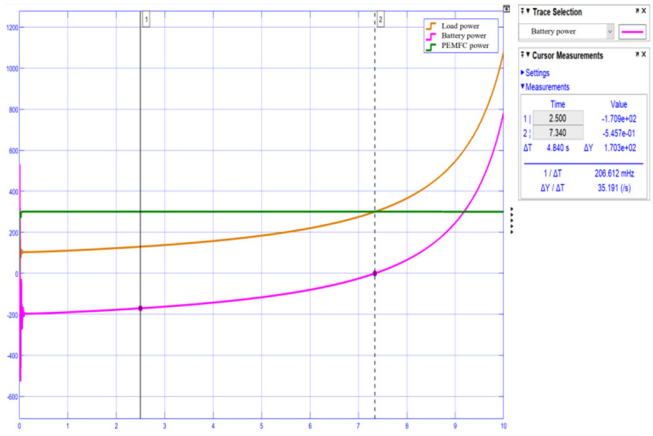

Fig. 11. Simulation results of interaction power components.

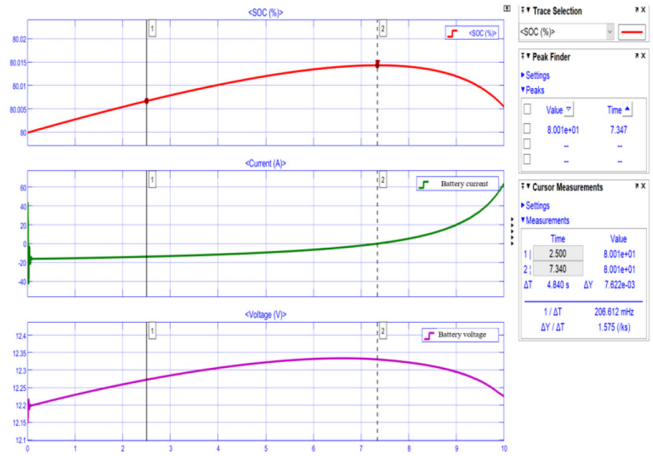

Fig. 12. Simulation results of battery operating parameter.

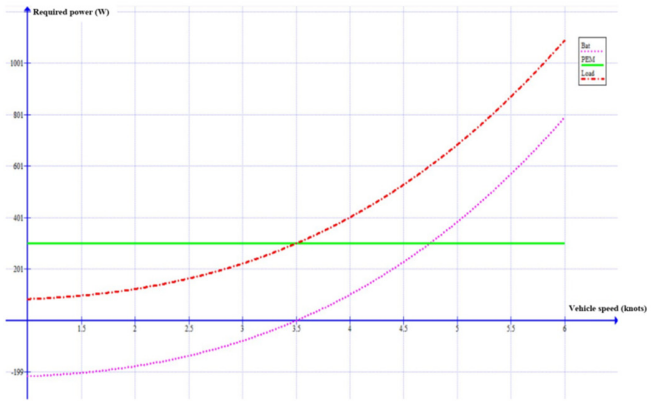

Fig. 13. Simulation results of power versus operating ROV speed.

IV. CONCLUSION

The theoretical basis for calculating the required power for UUV is based on the general method presented in [25]. The first novelty of this study is the proposal of fuel-cell hybrid propulsion with the required power of 300 W to replace the original battery propulsion.

The second novelty is the development of a data set for calculating the essential components of a fuel cell-based hybrid propulsion system, such as PEMFC, battery bank, fuel, oxygen flow, and DC-DC boost converter. These data are used as an input to understand the relationship between the FC parameters and the fuel cell-based hybrid propulsion during operation.

Other published works [13, 14] that reported creating fuel cell-based hybrid propulsion systems were based only on experience and the manufacturing of many prototypes. The present study highlighted this issue by building a model of the components of the dynamic system. Simulation conditions are periodically controlled, keeping the PEMFC's power supply stable, automating the PEMFC, making the system more accessible, and reducing manufacturing costs.

A final novelty is that the simulation results revealed the power interaction of the components in the dynamic system. This finding can be applied to diving vehicles in general and is the basis for improving the purely battery-electric propulsion system to a fuel cell-based hybrid propulsion system to increase the range and endurance of vehicles.

REFERENCES

[1] M. Fava, "How much of the Ocean has been explored?," *Ocean Literacy Portal*, May 09, 2022. https://oceanliteracy.unesco.org/ocean-exploration/.

[2] J.-C. Lee and T. Shay, "Analysis of Fuel Cell Applied for Submarine Air Independent Propulsion (AIP) System," *Journal of Marine Science and Technology*, vol. 26, no. 5, pp. 657–666, Oct. 2018, https://doi.org/10.6119/JMST.201810_26(5).0005.

[3] L. van Biert, M. Godjevac, K. Visser, and P. V. Aravind, "A review of fuel cell systems for maritime applications," *Journal of Power Sources*, vol. 327, pp. 345–364, Sep. 2016, https://doi.org/10.1016/j.jpowsour.2016.07.007.

[4] A. Mendez, T. J. Leo, and M. A. Herreros, "Current State of Technology of Fuel Cell Power Systems for Autonomous Underwater Vehicles," *Energies*, vol. 7, no. 7, pp. 4676–4693, Jul. 2014, https://doi.org/10.3390/en7074676.

[5] L. van Biert and K. Visser, "Chapter 3 - Fuel cells systems for sustainable ships," in *Sustainable Energy Systems on Ships*, F. Baldi, A. Coraddu, and M. E. Mondejar, Eds. Elsevier, 2022, pp. 81–121, https://doi.org/10.1016/B978-0-12-824471-5.00010-4.

[6] N. H. Hiep, N. Q. Quan, G. H. Thai, and P. T. San, "Numerical Modeling and Experimental Validation of a Hydrogen/Oxygen Fuel Cell for Underwater Vehicle Applications," SAE International, SAE Technical Paper 2023-01-5053, Aug. 2023, https://doi.org/10.4271/2023-01-5053.

[7] E. Di Gennaro, F. Baralli, E. Bovio, O. Faggioni, O. and M. Soldani, "Clearance Operation of Teulada Site (Italy): A Novel Approach for Short Term MCM Missions in Seafloor Hard Conditions," presented at the UDT Europe 2008 Conference, Jan. 2008.

[8] L. Carrette, K. A. Friedrich, and U. Stimming, "Fuel Cells – Fundamentals and Applications," *Fuel Cells*, vol. 1, no. 1, pp. 5–39, 2001, https://doi.org/10.1002/1615-6854(200105)1:1<5::AID-FUCE5>3.0.CO;2-G.

[9] H. N. Ha, Q. N. Quoc, and P. C. Xuan, "Early-Stage Analysis of Air Independent Propulsion Based on Fuel Cells for Small Submarines," *Advances in Military Technology*, vol. 17, no. 2, pp. 457–469, Nov. 2022, https://doi.org/10.3849/aimt.01744.

[10] C. Spiegel. *PEM Fuel Cell Modeling and Simulation Using Matlab.* Elsevier, 2008.

[11] B. Sundén, *Hydrogen, Batteries and Fuel Cells*. Academic Press, 2019.

[12] H. Weydahl, M. Gilljam, T. Lian, T. C. Johannessen, S. I. Holm, and J. Ø. Hasvold, "Fuel cell systems for long-endurance autonomous underwater vehicles – challenges and benefits," *International Journal of Hydrogen Energy*, vol. 45, no. 8, pp. 5543–5553, Feb. 2020, https://doi.org/10.1016/j.ijhydene.2019.05.035.

[13] N.-C. Shih, B.-J. Weng, J.-Y. Lee, Y.-C. Hsiao, "Development of a small fuel cell underwater vehicle," *International Journal of Hydrogen Energy,* vol. 38, no. 25, pp.11138-11143, Aug. 2013, https://doi.org/10.1016/j.ijhydene.2013.01.095.

[14] N.-C. Shih, B.-J. Weng, J.-Y. Lee, Y.-C. Hsiao, "Development of a 20 kW generic hybrid fuel cell power system for small ships and underwater vehicles", *International Journal of Hydrogen Energy*, vol. 39, no. 25, pp. 13894-13901, Aug. 2014. http://doi.org/10.1016/j.ijhydene.2014.01.113.

[15] N. H. Hiep and V. Duong, "Numerical and Experimental Investigation of Performance and Flooding Phenomena of a PEM Fuel Cell with and without Micro-Porous Layers," *Engineering, Technology & Applied Science Research*, vol. 14, no. 2, pp. 13444–13448, Apr. 2024, https://doi.org/10.48084/etasr.6996.

[16] A. Khadhraoui, T. Selmi, and A. Cherif, "Energy Management of a Hybrid Electric Vehicle," *Engineering, Technology & Applied Science Research*, vol. 12, no. 4, pp. 8916–8921, Aug. 2022, https://doi.org/10.48084/etasr.5058.

[17] D. Hidouri, R. Marouani, and A. Cherif, "Modeling and Simulation of a Renewable Energy PV/PEM with Green Hydrogen Storage," *Engineering, Technology & Applied Science Research*, vol. 14, no. 1, pp. 12543–12548, Feb. 2024, https://doi.org/10.48084/etasr.6492.

[18] S. Javadpoor and D. Nazarpour, "Modeling a PV-FC-Hydrogen Hybrid Power Generation System," *Engineering, Technology & Applied Science Research*, vol. 7, no. 2, pp. 1455–1459, Apr. 2017, https://doi.org/10.48084/etasr.760.

[19] M. A. Biberci and M. B. Celik, "Dynamic Modeling and Simulation of a PEM Fuel Cell (PEMFC) during an Automotive Vehicle's Driving Cycle," *Engineering, Technology & Applied Science Research*, vol. 10, no. 3, pp. 5796–5802, Jun. 2020, https://doi.org/10.48084/etasr.3352.

[20] J. Chakravorty, J. Saraswat, and V. Bhatia, "Modeling a Distributed Power Flow Controller with a PEM Fuel Cell for Power Quality Improvement," *Engineering, Technology & Applied Science Research*, vol. 8, no. 1, pp. 2585–2589, Feb. 2018, https://doi.org/10.48084/etasr.1807.

[21] G. De Lorenzo *et al.*, "Modelling and Performance Analysis of an Autonomous Marine Vehicle Powered by a Fuel Cell Hybrid Powertrain," *Energies*, vol. 15, no. 19, Jan. 2022, Art. no. 6926, https://doi.org/10.3390/en15196926.

[22] E. W. Saeed, E. G. Warkozek, "Modeling and analysis of renewable PEM fuel cell system," *Energy Procedia,* vol. 74, pp. 87–101, Aug. 2015, https://doi.org/10.1016/j.egypro.2015.07.527.

[23] S. A. Ansari, M. Khalid, K. Kamal, T. Abdul Hussain Ratlamwala, G. Hussain, and M. Alkahtani, "Modeling and Simulation of a Proton Exchange Membrane Fuel Cell Alongside a Waste Heat Recovery System Based on the Organic Rankine Cycle in MATLAB/SIMULINK Environment," *Sustainability*, vol. 13, no. 3, Jan. 2021, Art. no. 1218, https://doi.org/10.3390/su13031218.

[24] "Pluto PLUS ROV," *Gaymarine*. https://www.gaymarine.it/en/products/rov-pluto-plus.

[25] R. d'Amore-Domenech, M. A. Raso, A. Villalba-Herreros, Ó. Santiago, E. Navarro, and T. J. Leo, "Autonomous underwater vehicles powered by fuel cells: Design guidelines," *Ocean Engineering*, vol. 153, pp. 387–398, Apr. 2018, https://doi.org/10.1016/j.oceaneng.2018.01.117.